

# A direct method for analysing the nonlinear vehicle–structure interaction in high-speed railway lines

S.G.M. Neves<sup>a,b,\*</sup>, P.A. Montenegro<sup>b</sup>, A.F.M. Azevedo<sup>b</sup>, R. Calçada<sup>b</sup>

<sup>a</sup> ISEP, Polytechnic Institute of Porto, Rua Dr. António Bernardino de Almeida, 431, 4200-072 Porto, Portugal

<sup>b</sup> Centro de Estudos da Construção, Faculdade de Engenharia, Universidade do Porto, Rua Dr. Roberto Frias, 4200-465 Porto, Portugal

## ABSTRACT

The current maximum operating speed of trains on high-speed lines is 350 km/h and the maximum speed of 574.8 km/h was reached by a special TGV train in tests. Due to the increase of the train speed, taking into account the vehicle-structure interaction in the design process is essential to guarantee the serviceability of the bridge and the stability and running safety of the trains. Since in the design project, several trains running at tens of different speeds may have to be considered, resulting in hundreds of dynamic analyses, the efficiency of the methodology used is very important.

This article presents an accurate, efficient and robust computational procedure, referred to as the direct method, that can be used to analyse the nonlinear vehicle-structure interaction. The methods described in the literature and the currently available commercial software do not satisfy all the mentioned requirements. The direct method can be used in two or three dimensional problems and the subsystems that model the structure and vehicles may have any degree of complexity. The proposed methodology is implemented in MATLAB. The vehicles and structure are modelled with ANSYS, being the structural matrices subsequently imported by MATLAB.

The presented method establishes directly the equilibrium of the forces acting on the contact interface. The governing equilibrium equations of the vehicle and structure are complemented with

\* Corresponding author. Tel.: +351 228 340 500; fax: +351 228 321 159.

E-mail addresses: sgm.neves@fe.up.pt (S.G.M. Neves), pedro.montenegro@fe.up.pt (P.A. Montenegro), alvaro@fe.up.pt (A.F.M. Azevedo), ruiabc@fe.up.pt (R. Calçada).

additional constraint equations that relate the displacements of the nodes of the vehicle with the corresponding nodal displacements of the structure. These equations form a single system, with displacements and contact forces as unknowns, that is solved directly. The main advantage of establishing the direct equilibrium of forces, when compared with variational formulations, such as the Lagrange multiplier method, is a better understanding of the physical meaning of the equations. This is particularly important in complex problems such as the vehicle-structure interaction.

Due to the nonlinear nature of contact, an incremental formulation based on the Newton's method is adopted. A search algorithm is used to detect which elements are in contact, being the constraints imposed when contact occurs. In the normal direction the contact is modelled as a unilateral constraint problem and in the tangential direction frictionless sliding is allowed. A thorough understanding of the behaviour of the contact interface is essential. A nonlinear spring is used to model the normal contact, being the contact stiffness derived using the Hertz theory. Generally, a linearized value of the stiffness can be determined by considering the force-displacement relationship around the static wheel load. The influence of this linearization is studied in the present article.

The dynamic behaviour of a railway viaduct under the passage of the TGV double train is evaluated. Three-dimensional models are used and special attention is given to the viaduct and train dynamics. The service limit states, such as the riding comfort of the train, and the ultimate limit states, such as the track stability and the running safety of the vehicle are analysed. Finally, the fulfilment of some railway code requirements when considering trains travelling at high speeds and critical irregularities is investigated.

**Keywords:** vehicle-structure interaction, wheel-rail contact, high-speed train, bridges, nonlinear analysis

## **Abstract**

This article presents an accurate, efficient and stable algorithm to analyse the nonlinear vertical vehicle-structure interaction. The governing equilibrium equations of the vehicle and structure are complemented with additional constraint equations that relate the displacements of the vehicle with the corresponding displacements of the structure. These equations form a single system, with displacements and contact forces as unknowns, that is solved using an optimized block factorization algorithm. Due to the nonlinear nature of contact, an incremental formulation based on the Newton method is adopted. The track and structure are modelled using finite elements to take into account all the significant deformations. In the numerical example presented, the passage of the KHST over a railway viaduct is analysed, being the accuracy and computational efficiency of the proposed method clearly demonstrated.

**Keywords:** vehicle-structure interaction, wheel-rail contact, high speed train.

## **1 Introduction**

A vehicle-structure interaction problem is considerably more complex than a typical structural dynamics problem due to the relative movement between the two subsystems and the associated constraint equations relating the displacements of the vehicle and structure. In a significant number of studies available in the literature about the vehicle-structure interaction, the structure and vehicles are modelled as rigid multibody systems [1, 2]. Other authors, such as Antolín et al. [3] and Tanabe et al. [4], proposed formulations that additionally take into account the deformation of the structure. Neves et al. [5] modelled the vehicles and structure using finite elements, thus considering the deformation of both systems.

When the vehicle and structure are considered as a single system, the forces acting on the contact interface are internal forces. Since the vehicle moves relatively

to the structure, to avoid modifying the finite element mesh at each time step, Yang et al. [6] proposed a new contact element based on a condensation technique that eliminates the degrees of freedom at the contact interface. However, since the matrices of these elements depend on the position of the contact points, the global stiffness matrix is time-dependent and must be updated and factorized at each time step. This procedure may demand a considerable computational effort.

In the methods described in [7-10] the contact forces are considered explicitly but are not treated as unknowns of the governing equilibrium equations. In those works, an iterative procedure is used to ensure the coupling between the two subsystems. These methods may exhibit a slow rate of convergence, especially when unilateral contact is considered or a large number of contact points are required. To overcome these limitations, Neves et al. [5] developed an accurate, efficient and robust algorithm to analyse the vertical vehicle-structure interaction, referred to as the direct method, in which the governing equilibrium equations of the vehicle and structure are complemented with additional constraint equations that relate the displacements of the contact nodes of the vehicle with the corresponding nodal displacements of the structure, with no separation being allowed. These equations form a single system, with displacements and contact forces as unknowns, that is solved directly using an optimized block factorization algorithm.

In the present work an incremental formulation is used to take into account the nonlinear nature of contact. The time integration is performed using the  $\alpha$  method since it provides numerical dissipation in the higher modes while maintaining second-order accuracy [11]. The proposed methodology is implemented in MATLAB [12]. The vehicles and structure are modelled with ANSYS [13], being their structural matrices imported by MATLAB.

## 2 Contact and target elements

A two-dimensional node-to-segment contact element is used in the present formulation (see Fig. 1).

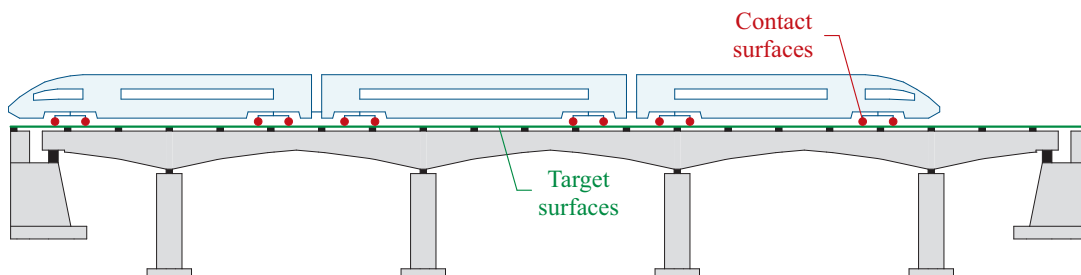


Figure 1: Contact pair concept.

In the direct method described in [5] no separation is allowed. In the present formulation a search algorithm is used to detect which elements are in contact, being the constraints imposed when contact occurs. Since in the present formulation only the frictionless contact is considered, the constraint equations are purely geometrical

and relate the displacements of the contact node with the displacements of the corresponding target element.

Figure 2 shows the two-dimensional node-to-segment contact element implemented in the present formulation and the local coordinate system  $(\xi_1, \xi_2, \xi_3)$  of the contact pair. The  $\xi_2$  axis always points towards the contact node, being the two elements separated by an initial gap  $g$ . The forces acting at the contact interface are denoted by  $X$  and the superscripts CE and TE indicate contact and target elements, respectively.

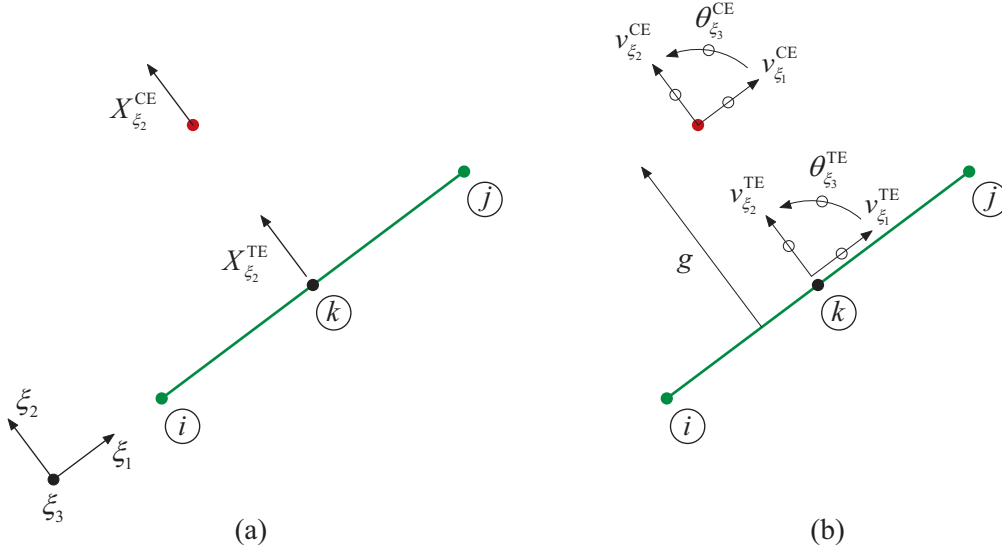


Figure 2: Node-to-segment contact element: (a) forces and (b) displacements at the contact interface.

According to Newton's third law, the forces acting at the contact interface must be of equal magnitude and opposite direction, i.e.,

$$\mathbf{X}^{CE} + \mathbf{X}^{TE} = \mathbf{0} \quad (1)$$

The displacement vector of an arbitrary point is defined by two translations,  $v_{\xi_1}$  and  $v_{\xi_2}$ , and a rotation  $\theta_{\xi_3}$  about the  $\xi_3$  axis. Since this type of contact element neglects the tangential forces and moments transmitted across the contact interface, the contact constraint equations only relate the displacement  $v_{\xi_2}$  of the contact node with the corresponding displacement of the auxiliary point  $k$ . Each constraint equation is defined in the local coordinate system of the contact pair and comprises the non-penetration condition for the normal direction. These equations are given by

$$\mathbf{v}^{CE} - \mathbf{v}^{TE} \geq -\mathbf{g} + \mathbf{r} \quad (2)$$

where  $\mathbf{r}$  are the irregularities of the contact interface. The gaps are always positive and a positive irregularity implies an increase of the distance between the contact and target elements (see Fig. 2).

### 3 Equations of motion

#### 3.1 Force equilibrium

The  $\alpha$  method is an implicit time integration scheme that is generally accurate and stable [11]. Assuming that the applied loads are deformation-independent and that the nodal point forces corresponding to the internal element stresses may depend nonlinearly on the nodal point displacements, the equations of motion of the vehicle-structure system given in [5] may be rewritten in the form

$$\mathbf{M}\ddot{\mathbf{a}}^{t+\Delta t} + \mathbf{C}\left[(1+\alpha)\dot{\mathbf{a}}^{t+\Delta t} - \alpha\dot{\mathbf{a}}^t\right] + (1+\alpha)\mathbf{R}^{t+\Delta t} - \alpha\mathbf{R}^t = (1+\alpha)\mathbf{F}^{t+\Delta t} - \alpha\mathbf{F}^t \quad (3)$$

where  $\mathbf{M}$  is the mass matrix,  $\mathbf{C}$  is the viscous damping matrix,  $\mathbf{R}$  are the nodal forces corresponding to the internal element stresses,  $\mathbf{F}$  are the externally applied nodal loads and  $\mathbf{a}$  are the nodal displacements. The superscripts  $t$  and  $t+\Delta t$  indicate the previous and current time steps, respectively.

To solve Eq. (3) let the  $F$  type degrees of freedom (d.o.f.) represent the free nodal d.o.f., whose values are unknown, and let the  $P$  type d.o.f. represent the prescribed nodal d.o.f., whose values are known. Thus, the load vector can be expressed as

$$\mathbf{F}_F = \mathbf{P}_F + \mathbf{D}_{FX}^{CE} \mathbf{X}^{CE} + \mathbf{D}_{FX}^{TE} \mathbf{X}^{TE} \quad (4)$$

$$\mathbf{F}_P = \mathbf{P}_P + \mathbf{D}_{PX}^{CE} \mathbf{X}^{CE} + \mathbf{D}_{PX}^{TE} \mathbf{X}^{TE} + \mathbf{S} \quad (5)$$

where  $\mathbf{P}$  corresponds to the externally applied nodal loads and  $\mathbf{S}$  are the support reactions. Each matrix  $\mathbf{D}$  relates the contact forces, defined in the local coordinate system of the respective contact pair, with the nodal forces defined in the global coordinate system (see Fig. 2).

Substituting Eq. (1) into Eqs. (4) and (5) leads to

$$\mathbf{F}_F = \mathbf{P}_F + \mathbf{D}_{FX} \mathbf{X} \quad (6)$$

$$\mathbf{F}_P = \mathbf{P}_P + \mathbf{D}_{PX} \mathbf{X} + \mathbf{S} \quad (7)$$

where

$$\mathbf{X} = \mathbf{X}^{CE} \quad (8)$$

$$\mathbf{D}_{FX} = \mathbf{D}_{FX}^{CE} - \mathbf{D}_{FX}^{TE} \quad (9)$$

$$\mathbf{D}_{PX} = \mathbf{D}_{PX}^{CE} - \mathbf{D}_{PX}^{TE} \quad (10)$$

Substituting Eqs. (6) and (7) into Eq. (3), and partitioning into  $F$  and  $P$  type d.o.f., gives

$$\mathbf{M}_{FF} \ddot{\mathbf{a}}_F^{t+\Delta t} + (1+\alpha)\mathbf{C}_{FF} \dot{\mathbf{a}}_F^{t+\Delta t} + (1+\alpha)\mathbf{R}_F^{t+\Delta t} - (1+\alpha)\mathbf{D}_{FX}^{t+\Delta t} \mathbf{X}^{t+\Delta t} = \bar{\mathbf{F}}_F \quad (11)$$

$$\begin{aligned} \mathbf{S}^{t+\Delta t} &= -\mathbf{P}_P^{t+\Delta t} - \mathbf{D}_{PX}^{t+\Delta t} \mathbf{X}^{t+\Delta t} \\ &+ \frac{1}{1+\alpha} \left[ \mathbf{M}_{PF} \ddot{\mathbf{a}}_F^{t+\Delta t} + \mathbf{M}_{PP} \ddot{\mathbf{a}}_P^{t+\Delta t} \right] + \mathbf{C}_{PF} \dot{\mathbf{a}}_F^{t+\Delta t} + \mathbf{C}_{PP} \dot{\mathbf{a}}_P^{t+\Delta t} + \mathbf{R}_P^{t+\Delta t} \\ &+ \frac{\alpha}{1+\alpha} \left[ \mathbf{S}^t + \mathbf{P}_P^t + \mathbf{D}_{PX}^t \mathbf{X}^t - \mathbf{C}_{PF} \dot{\mathbf{a}}_F^t - \mathbf{C}_{PP} \dot{\mathbf{a}}_P^t - \mathbf{R}_P^t \right] \end{aligned} \quad (12)$$

where

$$\begin{aligned} \bar{\mathbf{F}}_F &= (1+\alpha)\mathbf{P}_F^{t+\Delta t} - \alpha\mathbf{P}_F^t - \alpha\mathbf{D}_{FX}^t \mathbf{X}^t - \mathbf{M}_{FP} \ddot{\mathbf{a}}_P^{t+\Delta t} \\ &- (1+\alpha)\mathbf{C}_{FP} \dot{\mathbf{a}}_P^{t+\Delta t} + \alpha \left[ \mathbf{C}_{FF} \dot{\mathbf{a}}_F^t + \mathbf{C}_{FP} \dot{\mathbf{a}}_P^t \right] + \alpha \mathbf{R}_F^t \end{aligned} \quad (13)$$

### 3.2 Incremental formulation for nonlinear analysis

Since the present problem is nonlinear, Eq. (11) is rewritten in the form

$$\boldsymbol{\psi}(\mathbf{a}_F^{t+\Delta t}, \mathbf{X}^{t+\Delta t}) = \mathbf{0} \quad (14)$$

where  $\boldsymbol{\psi}$  is the residual force vector, given by

$$\begin{aligned} \boldsymbol{\psi}(\mathbf{a}_F^{t+\Delta t}, \mathbf{X}^{t+\Delta t}) &= \bar{\mathbf{F}}_F - \mathbf{M}_{FF} \ddot{\mathbf{a}}_F^{t+\Delta t} - (1+\alpha)\mathbf{C}_{FF} \dot{\mathbf{a}}_F^{t+\Delta t} - (1+\alpha)\mathbf{R}_F^{t+\Delta t} \\ &+ (1+\alpha)\mathbf{D}_{FX}^{t+\Delta t} \mathbf{X}^{t+\Delta t} \end{aligned} \quad (15)$$

The nodal velocities and accelerations depend on the nodal displacements and, for this reason, are not independent unknowns. In the  $\alpha$  method the velocity and acceleration at the current time step are approximated with

$$\dot{\mathbf{a}}^{t+\Delta t} = \frac{\gamma}{\beta\Delta t} (\mathbf{a}^{t+\Delta t} - \mathbf{a}^t) + \left(1 - \frac{\gamma}{\beta}\right) \dot{\mathbf{a}}^t + \Delta t \left(1 - \frac{\gamma}{2\beta}\right) \ddot{\mathbf{a}}^t \quad (16)$$

$$\ddot{\mathbf{a}}^{t+\Delta t} = \frac{1}{\beta\Delta t^2} (\mathbf{a}^{t+\Delta t} - \mathbf{a}^t) - \frac{1}{\beta\Delta t} \dot{\mathbf{a}}^t - \left(\frac{1}{2\beta} - 1\right) \ddot{\mathbf{a}}^t \quad (17)$$

where  $\beta$  and  $\gamma$  are parameters that control the stability and accuracy of the method.

An iterative scheme based on the Newton method [14] is used to solve Eq. (14). Assuming that the solution at the  $i$ th Newton iteration is already known and substituting Eqs. (16) and (17) into Eq. (14), leads to

$$\begin{aligned} & \boldsymbol{\Psi}(\mathbf{a}_F^{t+\Delta t, i}, \mathbf{X}^{t+\Delta t, i}) \\ & + \left[ -\frac{1}{\beta \Delta t^2} \mathbf{M}_{FF} - (1+\alpha) \frac{\gamma}{\beta \Delta t} \mathbf{C}_{FF} - (1+\alpha) \left[ \frac{\partial \mathbf{R}_F}{\partial \mathbf{a}_F^{t+\Delta t}} \bigg|_{\mathbf{a}_F^{t+\Delta t, i}} \right] \right] (\mathbf{a}_F^{t+\Delta t, i+1} - \mathbf{a}_F^{t+\Delta t, i}) \quad (18) \\ & + (1+\alpha) \mathbf{D}_{FX}^{t+\Delta t, i} (\mathbf{X}^{t+\Delta t, i+1} - \mathbf{X}^{t+\Delta t, i}) = \mathbf{0} \end{aligned}$$

Equation (18) can be rewritten as

$$\bar{\mathbf{K}}_{FF} \Delta \mathbf{a}_F^{i+1} - (1+\alpha) \mathbf{D}_{FX}^{t+\Delta t, i} \Delta \mathbf{X}^{i+1} = \boldsymbol{\Psi}(\mathbf{a}_F^{t+\Delta t, i}, \mathbf{X}^{t+\Delta t, i}) \quad (19)$$

being

$$\bar{\mathbf{K}}_{FF} = \frac{1}{\beta \Delta t^2} \mathbf{M}_{FF} + (1+\alpha) \frac{\gamma}{\beta \Delta t} \mathbf{C}_{FF} + (1+\alpha) \left[ \frac{\partial \mathbf{R}_F}{\partial \mathbf{a}_F^{t+\Delta t}} \bigg|_{\mathbf{a}_F^{t+\Delta t, i}} \right] \quad (20)$$

$$\Delta \mathbf{a}_F^{i+1} = \mathbf{a}_F^{t+\Delta t, i+1} - \mathbf{a}_F^{t+\Delta t, i} \quad (21)$$

$$\Delta \mathbf{X}^{i+1} = \mathbf{X}^{t+\Delta t, i+1} - \mathbf{X}^{t+\Delta t, i} \quad (22)$$

In matrix notation, Eq. (19) can be expressed as

$$\begin{bmatrix} \bar{\mathbf{K}}_{FF} & \bar{\mathbf{D}}_{FX} \end{bmatrix} \begin{bmatrix} \Delta \mathbf{a}_F^{i+1} \\ \Delta \mathbf{X}^{i+1} \end{bmatrix} = \boldsymbol{\Psi}(\mathbf{a}_F^{t+\Delta t, i}, \mathbf{X}^{t+\Delta t, i}) \quad (23)$$

with

$$\bar{\mathbf{D}}_{FX} = -(1+\alpha) \mathbf{D}_{FX}^{t+\Delta t, i} \quad (24)$$

After the evaluation of the solution at iteration  $i+1$ , the current residual force vector is calculated using Eq. (15). The iteration scheme continues until the following condition is fulfilled

$$\frac{\|\boldsymbol{\Psi}(\mathbf{a}_F^{t+\Delta t, i+1}, \mathbf{X}^{t+\Delta t, i+1})\|}{\|\mathbf{P}_F^{t+\Delta t}\|} \leq \varepsilon \quad (25)$$

being  $\varepsilon$  a specified tolerance.



## 4 Contact constraint equations

When contact occurs the non-penetration condition given by Eq. (2) is fulfilled if

$$\mathbf{v}^{CE} - \mathbf{v}^{TE} = -\mathbf{g} + \mathbf{r} \quad (26)$$

The displacements of the contact nodes (see Fig. 2) are given by

$$\mathbf{v}^{CE} = \mathbf{H}_{XF}^{CE} \mathbf{a}_F^{t+\Delta, i+1} + \mathbf{H}_{XP}^{CE} \mathbf{a}_P^{t+\Delta} \quad (27)$$

where each transformation matrix  $\mathbf{H}$  transforms the displacements of the contact nodes from the global coordinate system to the local coordinate system of the contact pair. The displacements of the auxiliary points of the target elements are given by

$$\mathbf{v}^{TE} = \mathbf{H}_{XF}^{TE} \mathbf{a}_F^{t+\Delta, i+1} + \mathbf{H}_{XP}^{TE} \mathbf{a}_P^{t+\Delta} \quad (28)$$

where each transformation matrix  $\mathbf{H}$  relates the nodal displacements of the target elements, defined in the global coordinate system, with the displacements of the auxiliary points defined in the local coordinate system of each contact pair.

Substituting Eqs. (27) and (28) into Eq. (26) yields

$$\mathbf{H}_{XF} \mathbf{a}_F^{t+\Delta, i+1} = -\mathbf{g} + \mathbf{r} - \mathbf{H}_{XP} \mathbf{a}_P^{t+\Delta} \quad (29)$$

where

$$\mathbf{H}_{XF} = \mathbf{H}_{XF}^{CE} - \mathbf{H}_{XF}^{TE} \quad (30)$$

$$\mathbf{H}_{XP} = \mathbf{H}_{XP}^{CE} - \mathbf{H}_{XP}^{TE} \quad (31)$$

Substituting Eq. (21) into Eq. (29) leads to

$$\mathbf{H}_{XF} \Delta \mathbf{a}_F^{i+1} = -\mathbf{g} + \mathbf{r} - \mathbf{H}_{XP} \mathbf{a}_P^{t+\Delta} - \mathbf{H}_{XF} \mathbf{a}_F^{t+\Delta, i} \quad (32)$$

Multiplying Eq. (32) by  $-(1+\alpha)$  gives

$$\bar{\mathbf{H}}_{XF} \Delta \mathbf{a}_F^{i+1} = \bar{\mathbf{g}} \quad (33)$$

where

$$\bar{\mathbf{H}}_{XF} = -(1+\alpha) \mathbf{H}_{XF} \quad (34)$$

and

$$\bar{\mathbf{g}} = -(1+\alpha) \left( -\mathbf{g} + \mathbf{r} - \mathbf{H}_{XP} \mathbf{a}_P^{t+\Delta t} - \mathbf{H}_{XF} \mathbf{a}_F^{t+\Delta t, i} \right) \quad (35)$$

Equations (23) and (33) can be expressed in matrix form leading to the following system of equations

$$\begin{bmatrix} \bar{\mathbf{K}}_{FF} & \bar{\mathbf{D}}_{FX} \\ \bar{\mathbf{H}}_{XF} & \mathbf{0} \end{bmatrix} \begin{bmatrix} \Delta \mathbf{a}_F^{i+1} \\ \Delta \mathbf{X}^{i+1} \end{bmatrix} = \begin{bmatrix} \boldsymbol{\psi}(\mathbf{a}_F^{t+\Delta t, i}, \mathbf{X}^{t+\Delta t, i}) \\ \bar{\mathbf{g}} \end{bmatrix} \quad (36)$$

## 5 Dynamic analysis of a railway viaduct

In order to validate the accuracy and efficiency of the proposed methodology a numerical example consisting of the Alverca railway viaduct subjected to the passage of the Korean high-speed train (KHST) is used. The results calculated using the direct method are compared with those obtained with the commercial software ANSYS [13]. In the analysis performed with the software ANSYS the Lagrange multiplier method is used.

### 5.1 Numerical model of the viaduct

The Alverca railway viaduct (see Fig. 3) is located at the km +18.676 of the Northern Line of the Portuguese railway network. The viaduct has a total length of 1091 m.

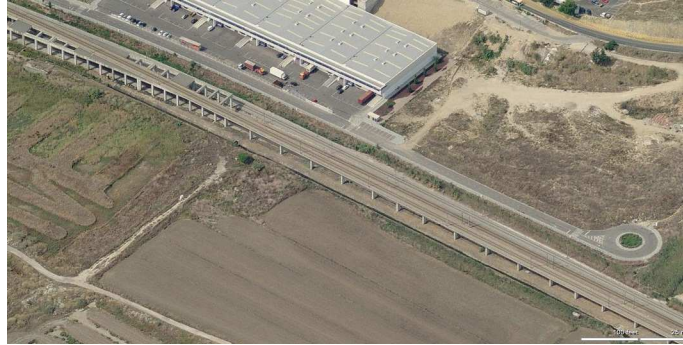


Figure 3: Aerial view of the viaduct.

The cross-section of the spans of the viaduct is shown in Fig. 4. Each span is composed of a prefabricated U-shaped prestressed beam and an upper slab casted in situ, which form a single-cell box-girder deck. The ballast retaining walls are monolithically connected to the upper slab of the deck.

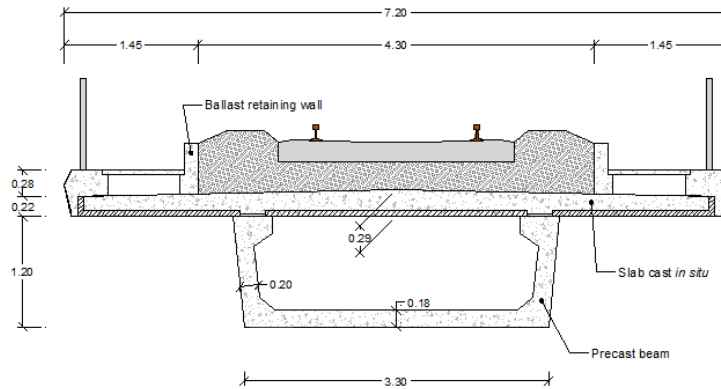


Figure 4: Cross-section of the viaduct.

Since the viaduct has several spans, the three-dimensional modelling of the complete viaduct using a personal computer would be impracticable due to the high computational cost. Therefore, only the three spans adjacent to the North abutment are modelled using the software ANSYS (see Fig. 5). An extension of the track with a length of 15 m was modelled to simulate the continuity of the track over the adjacent embankment. The U-shaped beams, the upper slabs and the ballast retaining walls are modelled with shell elements, and the ballast layer and sleepers with solid elements. Spring elements are used to model the rail pads and the supports of the spans, and the rails are modelled using beam elements. To take into account the non-structural elements, such as safeguards and edge beams, additional masses are considered. The model has 233292 unconstrained d.o.f. The calibration and experimental validation of the numerical model of the viaduct was performed by Malveiro *et al.* [15].

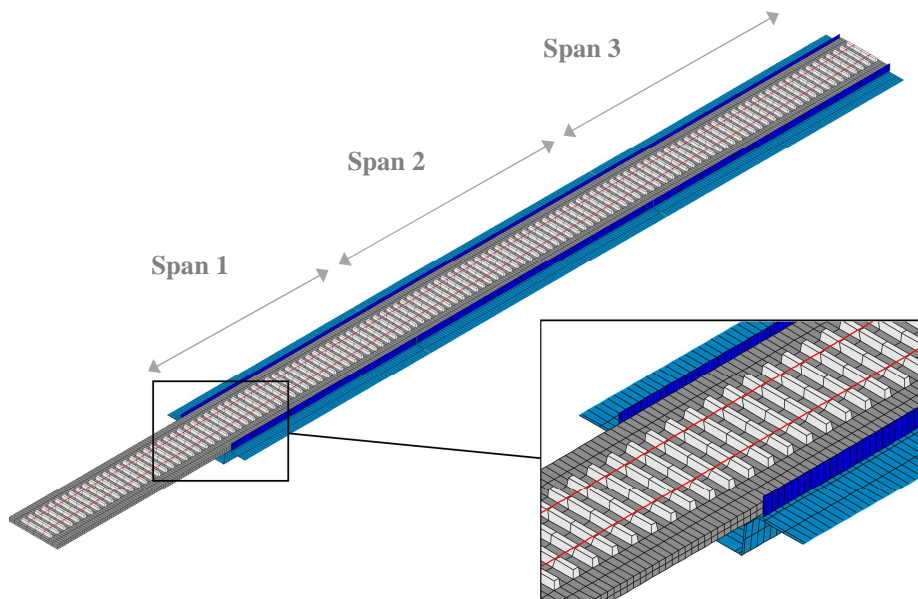


Figure 5: Numerical model of the first three spans of the viaduct.

The first four vertical vibration modes of the viaduct and the first torsional vibration mode are represented in Fig. 6 along with the corresponding natural frequencies.

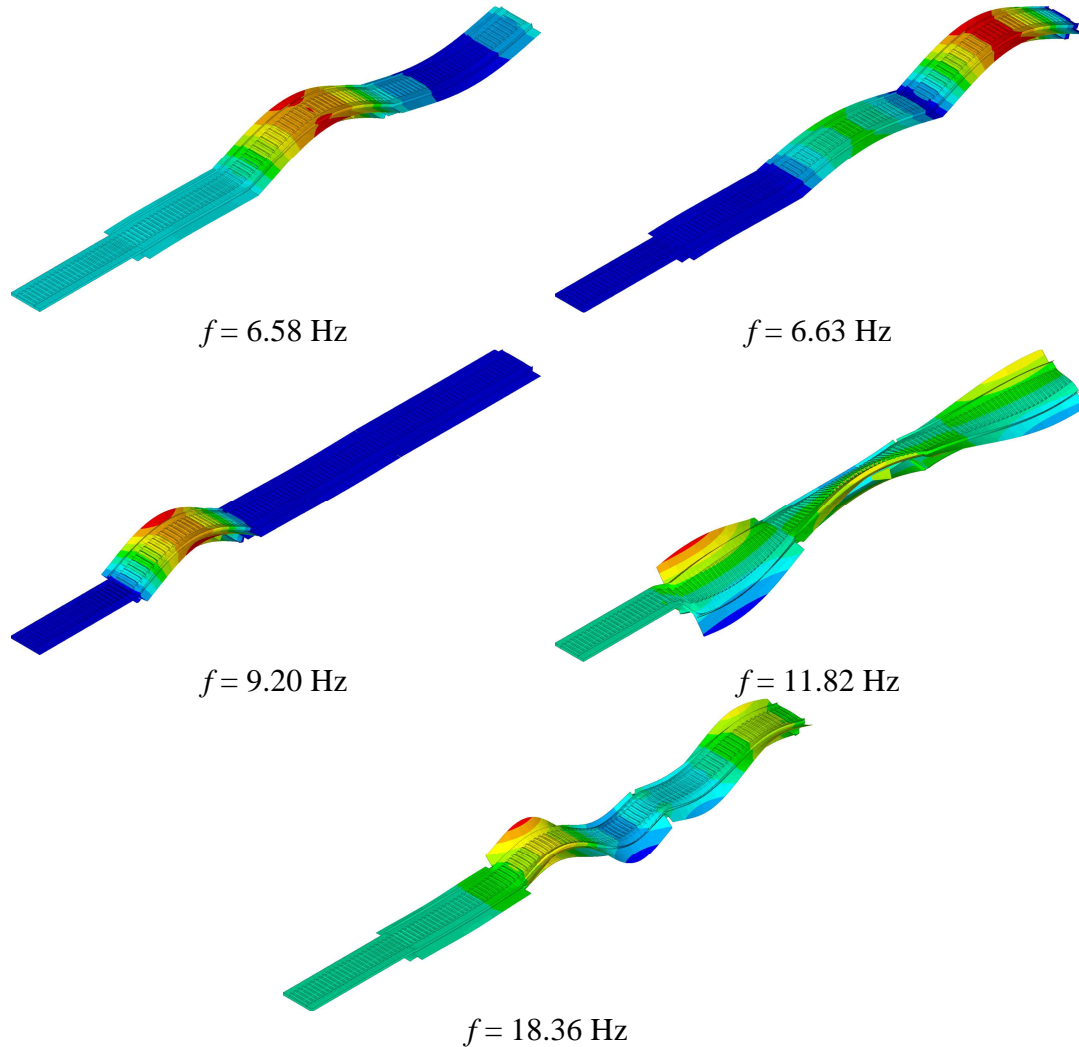


Figure 6: Global vibration modes and natural frequencies of the viaduct.

## 5.2 Numerical model of the train

The model of the KHST used in the present article is composed of two power cars on both ends connected to 16 passenger cars by means of two motorized trailers. The train has a total of 23 bogies and 46 axles, being the axle load at each wheelset of about 17 t. The total length between the first and last axles is 380.15 m.

The carbody, bogie frame and wheelset are considered as rigid bodies, and are modelled using point masses and rigid beam elements. The suspensions are modelled using spring-dampers in the three directions. The model has 8374

unconstrained d.o.f. The mechanical and geometrical properties of the vehicles are described in [16].

The numerical models of the power cars, motorized trailers and passenger cars are represented in Fig. 7, and the model of the bogies is depicted in more detail in Fig. 8.

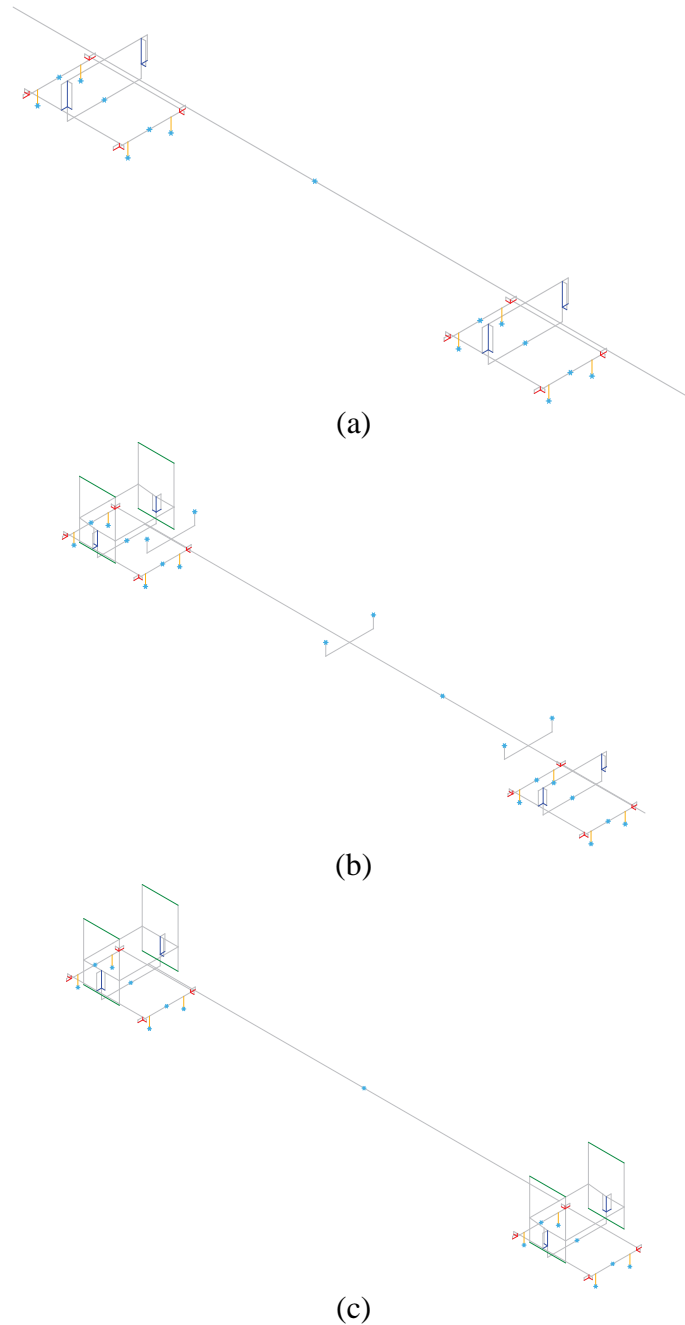


Figure 7: Numerical models of the train cars: (a) power car, (b) motorized trailer and (c) passenger car.

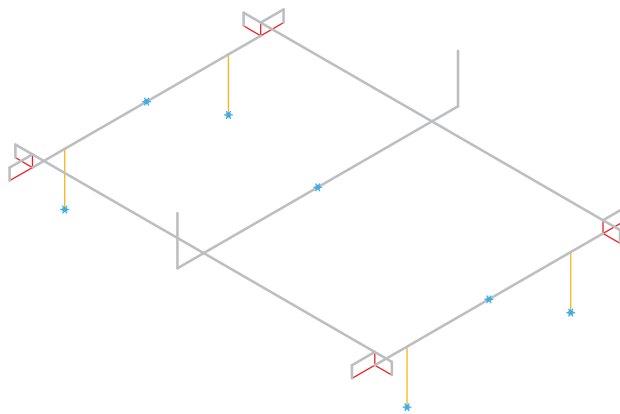


Figure 8: Numerical model of the bogie.

The first global vibration mode shapes and corresponding frequencies of the train are represented in Fig. 9.

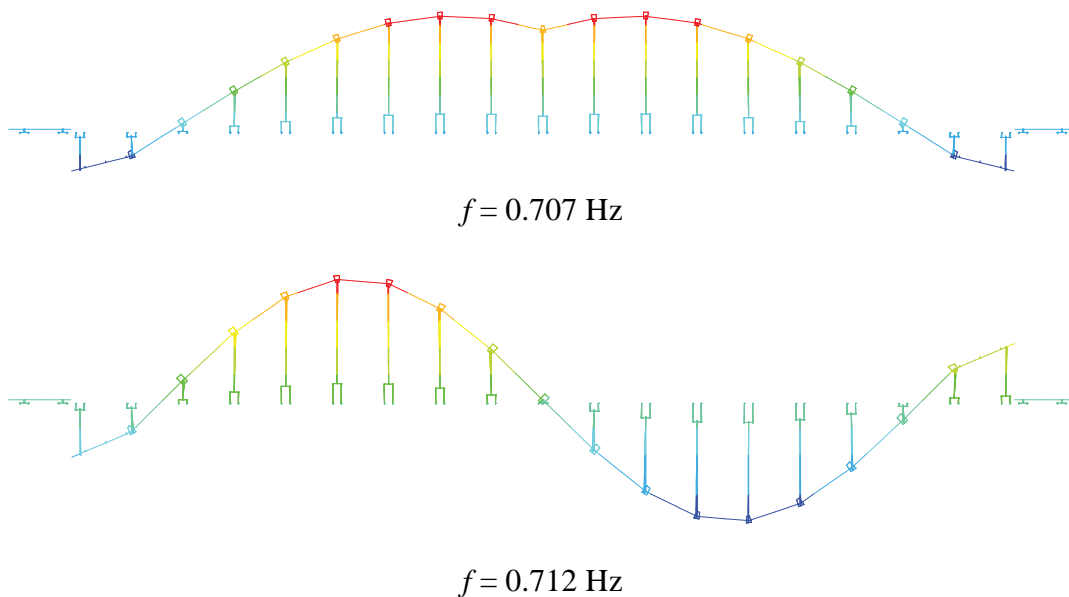


Figure 9: Global vibration modes and natural frequencies of the train.

### 5.3 Dynamic analysis

Since the total length between the first and last axles of the train is 380.15 m, modelling the complete track would greatly increase the computational cost of the analyses. Therefore, the train is initially supported by rigid beams (see Fig. 10) and the initial extension of the track is modelled as a critically damped system in order to damp out the sudden applied load of the train when it leaves the rigid beams.

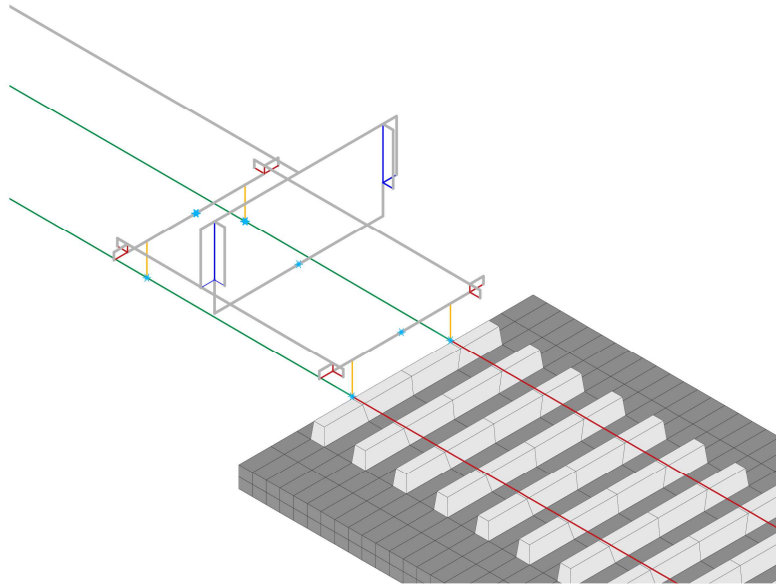


Figure 10: Initial rigid path supporting the train.

Since only the first three spans of the viaduct are modelled, the boundary conditions of the third span are not correctly taken into account and therefore only the passage of the train over the first two spans is analysed. The train travels at a constant speed of 120 m/s. A time step of  $2.5 \times 10^{-4}$  s is used and the total number of time steps is 2000. The following parameters for the  $\alpha$  method are considered:  $\alpha = -0.05$ ,  $\beta = 9/20$  and  $\gamma = 9025/40000$ .

The vertical accelerations at the midpoint of the second span, obtained with both the direct method and ANSYS, are plotted in Fig. 11.

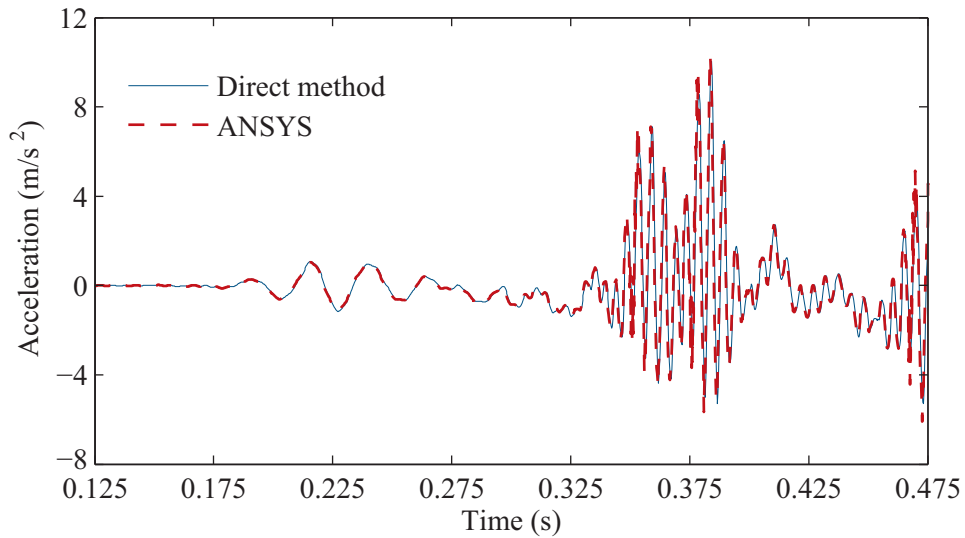


Figure 11: Vertical acceleration at the midpoint of the second span.

The vertical displacements of the first wheelset of the train are compared in Fig. 12. Finally, the accelerations of the carbody of the first power car are plotted in Fig.13.

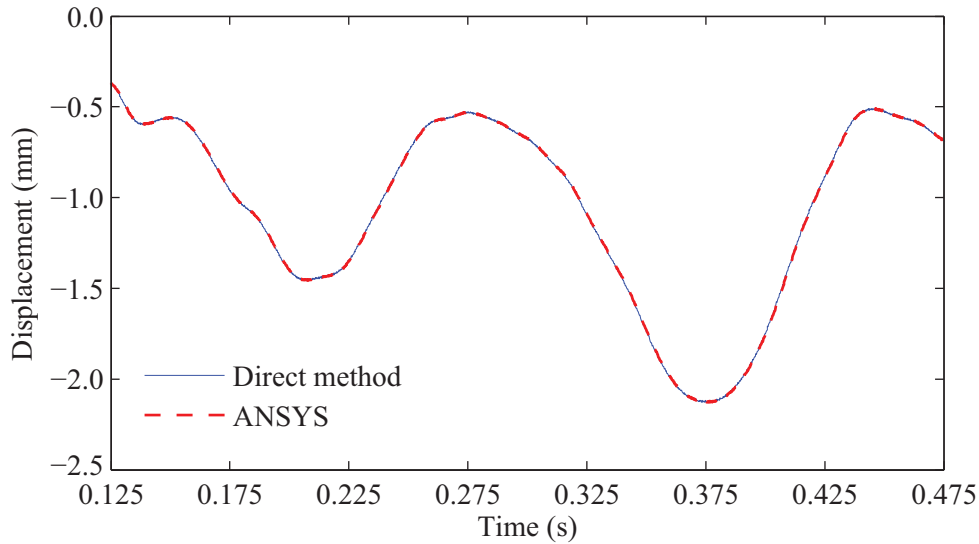


Figure 12: Vertical displacements of the first wheelset of the train.

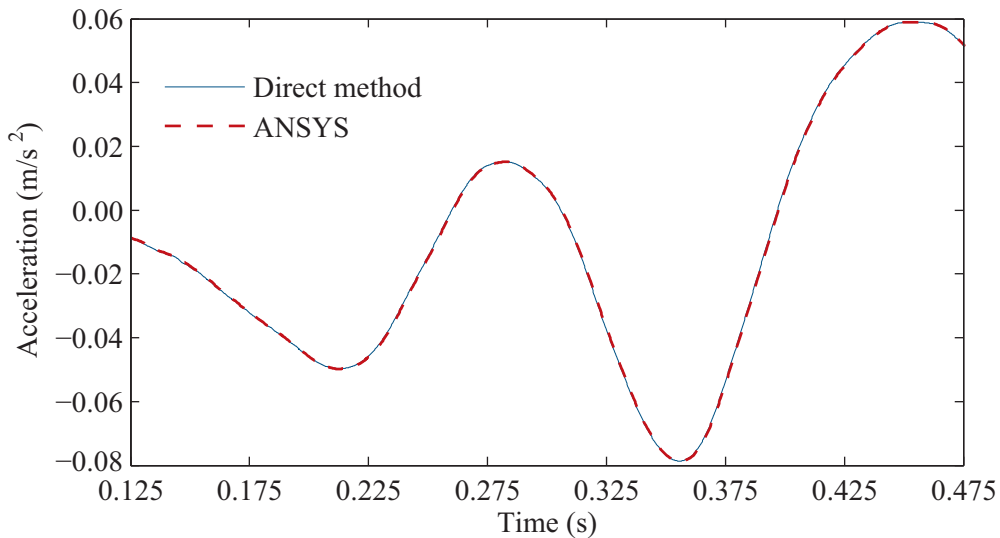


Figure 13: Vertical accelerations of the carbody of the first power car.

The results obtained with the direct method and the corresponding ANSYS solutions obtained using the classical Lagrange multiplier method show an excellent agreement.

All the calculations have been performed using a workstation with an Intel Xeon E5620 dual core processor running at 2.40 GHz. For a more accurate comparison, the calculations in ANSYS and MATLAB have been performed using a single



execution thread. The elapsed time is 34.3 hours using ANSYS and 5.7 hours using the direct method with the optimized block factorization algorithm, which is about six times faster.

## 6 Conclusions

An accurate, efficient and robust method for analysing the nonlinear vehicle-structure interaction is presented. The direct method is used to formulate the governing equilibrium equations and impose the constraint equations that relate the displacements of the contact node with the displacements of the corresponding target element. The accuracy of the method has been confirmed using a numerical example consisting of the passage of the KHST over a railway viaduct, in which the results obtained with the direct method and ANSYS show an excellent agreement.

The proposed method uses an optimized block factorization algorithm to solve the system of linear equations. The performed numerical analyses demonstrate the efficiency of the developed algorithm, since the calculations performed using the direct method are six times faster than the calculations performed with ANSYS.

Since in the present method the tangential creep forces acting at the interface are not considered, the lateral vehicle-structure interaction cannot be taken into account. To determine these forces, the material and geometric properties of the wheel and rail, and also the relative velocity between the two bodies at the contact point have to be considered. The extension of the present method to three-dimensional contact problems is under development and will be presented in a forthcoming publication.

## References

- [1] Pombo J, Ambrosio J, Silva M. A new wheel-rail contact model for railway dynamics, *Vehicle System Dynamics* 2007; 45: 165-189. DOI:10.1080/00423110600996017.
- [2] Shabana A, Zaazaa KE, Escalona JL, Sany JR. Development of elastic force model for wheel/rail contact problems, *Journal of Sound and Vibration* 2004; 269: 295-325. DOI:10.1016/S0022-460X(03)00074-9.
- [3] Antolín P, Goicolea JM, Oliva J, Astiz MA. Nonlinear train-bridge lateral interaction using a simplified wheel-rail contact method within a finite element framework, *Journal of Computational and Nonlinear Dynamics* 2012; 7: art. no. 041014. DOI:10.1115/1.4006736.
- [4] Tanabe M, Matsumoto N, Wakui H, Sogabe M, Okuda H, Tanabe Y. A simple and efficient numerical method for dynamic interaction analysis of a high-speed train and railway structure during an earthquake, *Journal of Computational and Nonlinear Dynamics* 2008; 3: art. no. 041002. DOI:10.1115/1.2960482.
- [5] Neves SGM, Azevedo AFM, Calçada R. A direct method for analyzing the vertical vehicle-structure interaction, *Engineering Structures* 2012; 34: 414-420. DOI:10.1016/j.engstruct.2011.10.010.

- [6] Yang YB, Wu YS. A versatile element for analyzing vehicle-bridge interaction response, *Engineering Structures* 2001; 23: 452-469. DOI:10.1016/S0141-0296(00)00065-1.
- [7] Delgado R, Santos SM. Modelling of railway bridge-vehicle interaction on high speed tracks, *Computers & Structures* 1997; 63: 511-523. DOI:10.1016/S0045-7949(96)00360-4.
- [8] Lei X, Noda NA. Analyses of dynamic response of vehicle and track coupling system with random irregularity of track vertical profile, *Journal of Sound and Vibration* 2002; 258: 147-165. DOI:10.1006/jsvi.2002.5107.
- [9] Nguyen D-V, Kim K-D, Warnitchai P. Dynamic analysis of three-dimensional bridge-high-speed train interactions using a wheel-rail contact model, *Engineering Structures* 2009; 31: 3090-3106 DOI:10.1016/j.engstruct.2009.08.015.
- [10] Yang F, Fonder G. An iterative solution method for dynamic response of bridge-vehicles systems, *Earthquake Engineering and Structural Dynamics* 1996; 25: 195-215. DOI:10.1002/(SICI)1096-9845(199602)25:2<195::AID-EQE547>3.0.CO;2-R.
- [11] Hilber HM, Hughes TJR, Taylor RL. Improved numerical dissipation for time integration algorithms in structural dynamics, *Earthquake Engineering & Structural Dynamics* 1977; 5: 283-292. DOI:10.1002/eqe.4290050306.
- [12] MATLAB<sup>®</sup>. R2013b, The MathWorks Inc., Natick, MA; 2013.
- [13] ANSYS<sup>®</sup>. Academic Research, Release 14.5, ANSYS Inc., Canonsburg, PA; 2013.
- [14] Owen DRJ, Hinton E. *Finite elements in plasticity: Theory and practice*. Pineridge Press Limited, Swansea, UK; 1980.
- [15] Malveiro J, Ribeiro D, Calçada R, Delgado R. Updating and validation of the dynamic model of a railway viaduct with precast deck, *Structure and Infrastructure Engineering* 2013; 1-26. DOI:10.1080/15732479.2013.833950.
- [16] Kwark JW, Choi ES, Kim YJ, Kim BS, Kim SI. Dynamic behavior of two-span continuous concrete bridges under moving high-speed train, *Computers & Structures* 2004; 82: 463-474.